ORIGINAL ARTICLE

Application of spindle power signals in tool condition monitoring based on HHT algorithm

Bin Shen[1] · Yufei Gui[1] · Biao Chen[1] · Zichao Lin[1] · Qi Liu[1] · Qizheng Liu[1]

Abstract

In the present study, we present the application of spindle power signals in tool condition monitoring (TCM) under different cutting conditions based on the Hilbert-Huang transform (HHT) algorithm. We extracted two features from the original collected data using the HHT algorithm to detect the tool wear and conducted six sets of cutting experiments to verify the feasibility of this tool condition monitoring method. The results show that these features are highly correlated with the wear state of cutting tools, regardless of the cutting parameters, workpiece materials, and machining methods. The calculated correlation coefficients between the extracted features and the actual tool wear reach 0.79–0.98. This demonstrates that the HHT algorithm is suitable for extracting features from the spindle power signals to construct the online tool condition monitoring system.

Keywords Tool condition monitoring (TCM) · Spindle power signal · Hilbert-Huang transform (HHT)

1 Introduction

Machining is a highly complicated process that is significantly affected by a variety of combinations of cutting parameters [1, 2], different machinability of materials [3, 4], diverse mechanisms of machining methods [5–7], and varying design strategies of tools [8, 9]. Among them, the cutting tool is one of the most critical factors of determining the products' quality and machining efficiency. During a cutting process, wear occurs on the cutting edge of the cutting tool due to the thermal fracturing, abrasion, adhesion, diffusion, or chemical wear, and the cutting edge inevitably becomes blunt gradually [10]. The cutting tool with blunt cutting edges leads to unwanted vibration, which deteriorates the surface finish and causes dimensional inaccuracy [11]. Therefore, the implementation of online tool condition monitoring (TCM) in real-time during a cutting process is highly critical for producing high-quality parts and improving the production efficiency in industrial practice.

Challenges remain on establishing an accurate and low-cost online tool condition monitoring (TCM) system. Currently, the reported TCM systems can be classified into two categories, namely the direct-monitoring and the indirect-monitoring system [12]. The direct-monitoring system monitors the tool condition by measuring changes occurred in the actual shape or surface of cutting tools during the cutting process via the radiation, electric resistance, optical system, etc. It cannot implement the real-time monitoring due to the continuous contact between the cutting tool and the workpiece and the presence of coolant fluids [13]. The indirect-monitoring system evaluates the tool condition by analyzing one or several signals, such as the spindle power, cutting force, vibration, and AE, which closely relates with the tool condition and can be collected at a low cost during the cutting process [10, 14, 15]. Using the spindle power as the source signal has many advantages. Collecting the spindle power of the machine tool in the cutting process is rather simple and does not require any modification on the machine tool or customization on fixtures, which makes it possible to implement a low-cost and real-time online monitoring process. However, compared with other signals, the spindle power signal collected during the cutting process contains much more noise since it is susceptible to severe viscous drag and friction between mechanical structures [13]. Therefore, one critical step of constructing a feasible TCM system based on the spindle power signal is finding an algorithm that

✉ Bin Shen
binshen@sjtu.edu.cn

1 School of Mechanical Engineering, Shanghai Jiao Tong University, Shanghai 200240, China

can effectively filter the raw spindle power signals and extract at least one feature to reflect the tool condition precisely.

Instead of the time domain or frequency domain analysis, time-frequency analysis methods, such as the wavelet transform (WT) [16, 17] and the Hilbert-Huang transform (HHT) [12, 18], are widely used to analyze the nonlinear and nonstationary spindle power signal collected from the cutting process. Based on the WT algorithm, Shao et al. [19] decomposed the single-channel spindle power signal into several groups of signals, from which the signals related to a milling cutter and spindle were separated. Choi et al. [20] used the WT algorithm to obtain details of the cutting force signal and estimate trends of the tool wear. In practice, the WT can only be used to postprocess the linear nonstationary signals as the selection and construction of the wavelet bases are challenging and highly depend on the cutting conditions.

The Hilbert-Huang transform (HHT) algorithm is a novel signal analysis method derived by Huang et al. [21]. It consists of the empirical mode decomposition (EMD) and the intrinsic mode function (IMF). It decomposes signals according to their time-scale features without any basis functions. Therefore, theoretically, it can be used to analyze any nonlinear and nonstationary signal, including the spindle power signal collected in the cutting process, because both the harmonic component and noises could be suppressed effectively in this way. Several studies had attempted to utilize the HHT algorithm to construct online TCM systems. For example, Bassiuny et al. [22] used smooth nonlinear energy operators and the HHT to capture characteristics of the motor current signal and predict the tool breakage successfully. Raja et al. [23] found that the tool wear would lead to an increase in the amplitude of the corresponding IMF component when they employed the HHT to process AE signals in the turning process. Sun et al. [24] developed a TCM system by extracting features from vibration signals using HHT algorithm and inputting eigenvectors to the neural network to judge the tool wear status. However, the development of an online TCM system based on the analysis of spindle power signals using the HHT algorithm has not been reported.

In the present study, based on the HHT algorithm, we extracted a feature from the spindle power signals that can precisely reflect the tool condition in real-time, which makes it possible to develop an effective and low-cost online TCM system based on the spindle power signal. We constructed a spindle power signal acquisition system using sensors, DAQ, and Lab VIEW and extracted the suitable feature (η) from the signal based on the HHT algorithm. As available studies had demonstrated the effectiveness and accuracy of the continuous wavelet transform (CWT) algorithm in the feature extraction [25–27]we processed the raw spindle power signals using both the CWT and HHT algorithm and compare the obtained results to demonstrate both the advantages and disadvantages of the method proposed in the present study. The correlation coefficient value (r) between the extracted feature (η) and the measured tool flank wear (VB) is used as the index to evaluate the prediction accuracy of the algorithm used in the analysis. Besides, we demonstrated the feasibility of monitoring the tool condition by analyzing the spindle power signal using the HHT algorithm in a set of well-designed cutting experiments.

2 Experimental

In the present study, we adopted the HHT algorithm to analyze the spindle power signal and obtained two features (η_1 and η_2) that closely relate to the tool condition. For the sake of comparison, we also used the CWT algorithm to generate another feature (η_0) from the same raw data. We provide a detailed description on the extraction of these features, as well as the setup of cutting experiments.

2.1 Spindle power signal processing

2.1.1 Feature extraction using the CWT algorithm

The CWT algorithm, which was developed from the Fourier transform, is a time-frequency domain analysis method that applies to process the nonstationary signal. The most critical step for implementing CWT algorithm is to choose an optimal wavelet basis function that well matches the waveform of a specific original signal. Based on the frequency spectrum of the raw data and the property of the wavelet function, we choose the complex Morlet wavelet basis functions "cmor3-3" with a bandwidth of 3 and a center frequency of 3 [28]. The CWT decomposes the raw signal into a linear combination of these basis functions. Figure 1a shows a CWT time-frequency spectrum. The magnitude of each CWT coefficient is represented by the brightness of each point in the time-frequency plane. The distinct white line of 133.3 Hz in the figure indicates that the energy of spindle power distributes around this frequency and the behavior of these maxima is strongly influenced by the wear of cutting tools. For this reason, these wavelet coefficients are considered as the optimal indicators, and the average values of them is defined as the feature (η_0) reflecting the tool condition. Figure 1b presents a flowchart of the whole extraction process.

2.1.2 The HHT algorithm

The HHT algorithm consists of two fundamental parts, namely, the empirical mode decomposition (EMD) and the Hilbert spectral analysis [21]. Using the EMD method, the raw signal is decomposed into a series of IMF components and a residue.

Fig. 1 **a** Wavelet time-frequency spectrum. **b** The flowchart of η_0 extraction
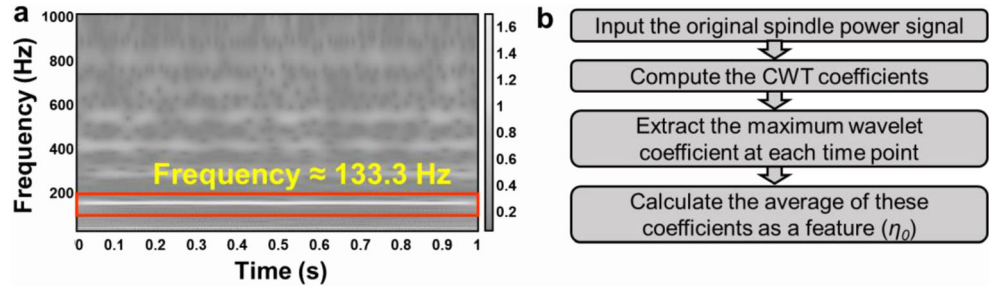
Then, the Hilbert transform is used to process each IMF to obtain the instantaneous frequency and amplitude of every moment.

Firstly, the original signal is decomposed into n intrinsic modes and a residue r_n:

$$x(t) = \sum_{i=1}^{n} c_i(t) + r_n(t) \tag{1}$$

The following step is to perform the Hilbert transform on each IMF. For any real value function $x(t)$ of L^p class, the Hilbert transform is essentially a convolution with the function $h(t) = \frac{1}{\pi t}$. Thus, the Hilbert transform of each IMF is defined as

$$Y_i(t) = \frac{P}{\pi} \int_{-\infty}^{\infty} \frac{c_i(\tau)}{t-\tau} d\tau \tag{2}$$

where P indicates the principal value of the singular integral. Then the analytic signal is defined as

$$Z(t) = X(t) + jY(t) = a(t)e^{j\theta(t)} \tag{3}$$

where

$$a(t) = \sqrt{X(t)^2 + Y(t)^2} \text{ and } \theta(t) = \arctan \frac{Y(t)}{X(t)} \tag{4,5}$$

Here, $a(t)$ denotes the instantaneous amplitude, $\theta(t)$ denotes the phase function, and the instantaneous frequency is naturally denoted by

$$\omega(t) = \frac{d\theta}{dt} \tag{6}$$

After the Hilbert transforming process, we obtain the Hilbert spectrum of the original signal as the following form:

$$H(\omega, t) = \text{Re} \sum_{i=1}^{n} a_i(t)e^{j\theta(t)} = \text{Re} \sum_{i=1}^{n} a_i(t)e^{j\int \omega_i(t)dt} \tag{7}$$

This expression illustrates that the Hilbert spectrum can be represented in a three-dimensional plot showing the amplitude distribution over time and frequency. Since the frequency and amplitude are both functions of time, we define the marginal spectrum as

$$h(\omega) = \int_0^T H(\omega, t)dt \tag{8}$$

The marginal spectrum is represented in a two-dimensional plot with the frequency and the amplitude. The amplitude of a specific frequency in the marginal spectrum displays the energy of the component corresponding to this frequency in the overall data. In terms of statistics, the larger the amplitude is, the higher the probability of the corresponding signal is. Unlike the Fourier transform using the whole periodic signal to determine the local frequency, the Hilbert transform directly defines the instantaneous frequency as a function of time, through which the local frequency properties of nonstationary signals are well preserved.

### 2.1.3 Feature extraction using the HHT algorithm

We extract two features from the raw spindle power signal by adopting the HHT algorithm. Firstly, the EMD is performed on the raw data to obtain seven IMF components and a residue r_7, as shown in Fig. 2a. These components have specific physical meanings. For example, the first few ones mainly correspond to high-frequency noises. Therefore, there should exist an optimal IMF component which can provide useful information about the state of tool wear. The presence of the energy peak in the frequency spectrum or marginal spectrum of the raw signal also supports this deduction. We signify the corresponding frequency as dominant frequency f_d.

During a stable cutting process like flank milling, the cutting force acted on the cutting tool varies periodically; thus, the dominant frequency should be equal to the tooth passing frequency (f_t), which is determined using the following equation:

$$f_t = k * \frac{n}{60} \tag{9}$$

where n is the spindle rotating velocity (rpm) and k is the number of teeth of the cutter.

We select the IMF component corresponding to f_d as an optimal one. The average absolute values of its extrema are denoted as a feature (η_1), which reflects the changes in the spindle power caused by the tool wear. The raw power signal in Fig. 2a is captured from a flank milling process. The spindle
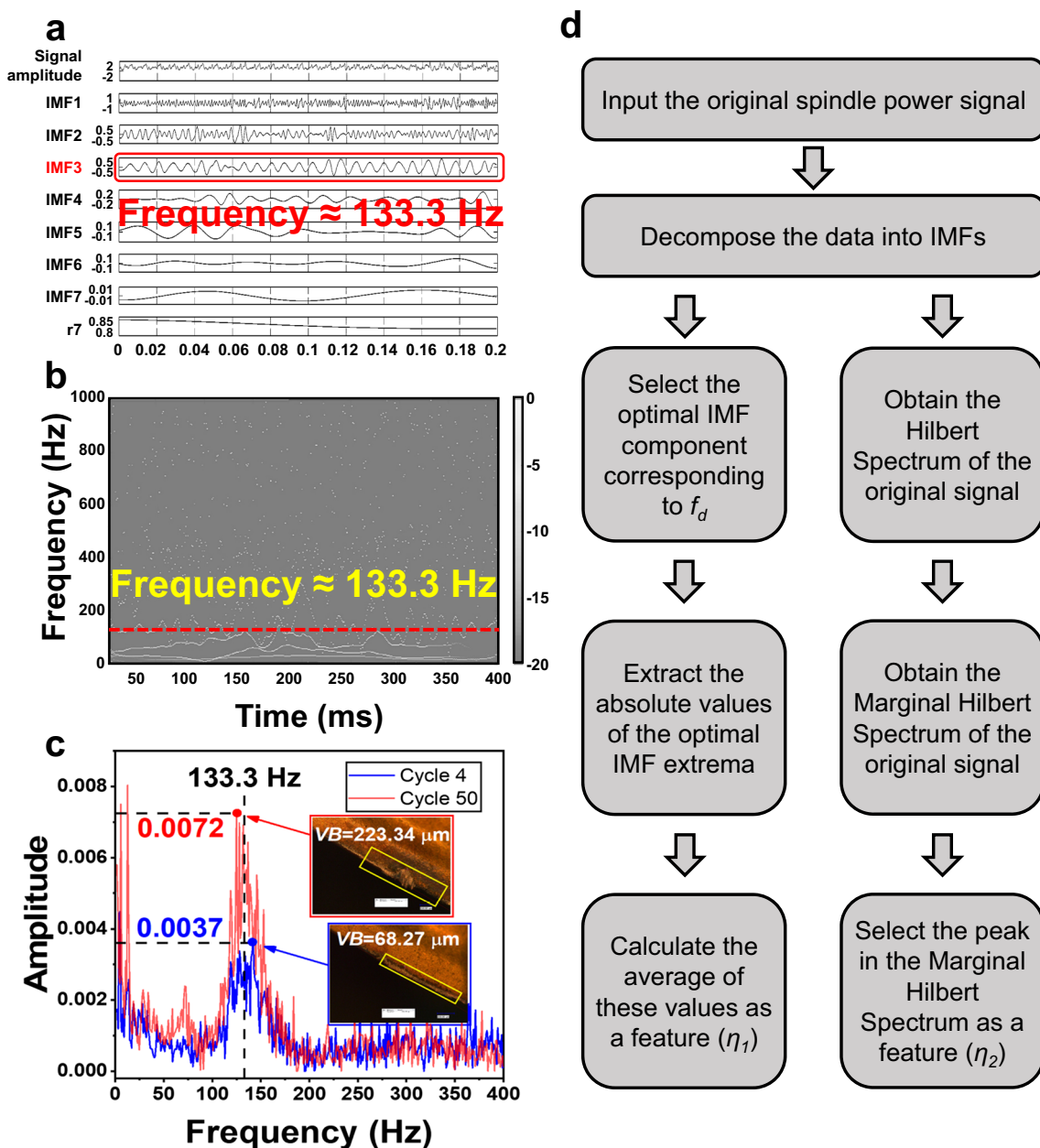
Fig. 2 **a** IMF components. **b** Hilbert-Huang spectrum of the 4th cutting cycle. **c** Marginal spectra of the 4th and 50th cutting cycle. **d** The flowchart of extracting η_1 and η_2

rotational speed is 8000 rpm. Only one tooth is installed. According to Eq. (9), f_t is 133.3 Hz, which is approximately equal to the frequency of IMF3. Therefore, we calculate η_1 based on this component.

Considering the insufficient performance of the EMD method on noise reduction, a certain amount of noise still exists in all the IMF components, including the optimal one. Therefore, η_1 might not be reliable enough in reflecting the geometric change of the cutting tool. As a reference, the Hilbert transform is performed on every IMF to generate the Hilbert-Huang spectrum and marginal spectrum, from which we can obtain another feature (η_2).

In this way, the influence of the tool wear on the spindle power can be characterized by the magnitude of peak in the spectrum, which is designated as η_2. In this test, the milling operations were performed repeatedly. Figure 2b shows the Hilbert spectrum of the 4th cutting cycle and Fig. 2c presents the marginal spectra and pictures of the tool edge in cycle 4 and 50. During the cycle 4, the tool is slightly worn with a flank wear of 0.07 mm, which reaches 0.22 mm after 46 cycles. In the marginal spectrum, the magnitude of the dominant component increases from 0.0037 to 0.0072 with a growth rate of 94.6%, while other harmonics are unaffected. This result indicates that the peak in the marginal spectrum is a reliable

indicator of the flank wear of the cutting tool. Figure 2d presents a flowchart of extracting the η_1 and η_2.

2.2 Experimental setup

We conducted a set of cutting experiments to verify the accuracy of the features extracted from spindle power signals based on the HHT algorithm in evaluating the tool condition under various machining conditions, in which we choose a variety of cutting parameters, workpiece materials, and machining methods. The cutting conditions are provided in Table 1. All tests were performed on a three-axis CNC drilling center. This machine tool has a maximum spindle power of 5.5 kW and a rotational speed of 20000 rpm. A Sandvik CoroMill390 with single coated carbide insert was used in flank milling experiments, which simplified the measurement of tool wear. An uncoated carbide drill bit and a TiN-coated drill bit were chosen for experiments 5 and 6, respectively. The average flank wear of two cutting edges represented the actual wear of the drill. In each cutting test, the cutting tool was unloaded from the spindle every 1–3 cutting passes and its flank wear was measured in a microscope. The lifetime of a cutting tools is defined as the cutting time it experienced before its flank wear reached 0.2 mm.

Figure 3 shows the spindle power signal acquisition system adopted in the present study. The current sensor and voltage sensor were mounted on the spindle motor cable to collect the current and voltage data, which were used to calculate the spindle power. The collected signals were digitalized by DAQ devices and stored in the local PC using a Lab View program. The accuracy of the voltage and current sensor was ± 6 V (measurement range, 0~ ± 900 V) and ± 1 A (measurement range, 0~ ± 150A). The DAQ device is a NI 9239 with a 24-bit resolution. The sampling rate of this acquisition system was 2 kHz. It means more than 12,500 data points were collected in one cutting pass (cutting length, 100 mm) with the fastest feed rate (960 mm/min) in the test. Due to the intermittency of the flank milling process, the collected signals carry useful information related with the cutting tool condition only when the cutting tool is in contact with the workpiece. Therefore, the signals between the time points corresponding to engagement and disengagement of the cutting tool and workpiece are selected as the raw data, from which we obtain the feature (η) reflecting the tool condition.

3 Experimental results

We processed the power signal collected from experiment 1 using the CWT and HHT algorithm separately. The results are presented in Fig. 4a, b, and c. Figure 4a represents the results obtained from the CWT method and the other two represent the results derived from the HHT method. The *VB* versus cutting cycle curve, as displayed in Fig. 4d, represents the typical variation pattern of the tool wear.

It is seen from Fig. 4a that the η_0 shows random distribution as a function of the cutting cycle. The correlation coefficient between the η_0 and VB is 0.34, indicating that the CWT algorithm failed to filter the noise in raw power signal effectively. In Fig. 4b, we can observe that the variation of η_1 is not consistent with that of the VB of the cutting tool neither. The correlation coefficient between the η_0 and VB is as low as 0.62, which is insufficient for reflecting the tool condition. However, a turning point presents near the 45th cutting cycle, where the VB of the cutting tool is about 0.15 mm, which corresponds the critical point at which the tool condition transfers from the normal wear region to the rapid wear regime. Comparatively, in Fig. 4c, it appears that the η_2 coincides with the VB variation well during the whole cutting test,

Table 1 Cutting conditions

Experiment	Tool (insert)	Rotational speed (r/min)	Cutting depth (mm)	Cutting width (mm)	Feed rate (mm/min)	f_t (Hz)	Machining method	Workpiece material
1	2030	8000	2	3	800	133.3	Flank milling	45 steel
2	2030	8000	3	3	960	133.3	Flank milling	45 steel
3	2030	6000	2	4	600	100	Flank milling	45 steel
4	S30T	1200	2	4	96	20	Flank milling	TC4
5	Uncoated	6000	–	–	960	200	Drilling	45 steel
6	TiCN coating	1600	–	–	160	53.3	Drilling	TC4

Fig. 3 Experimental setup: spindle power signal acquisition system
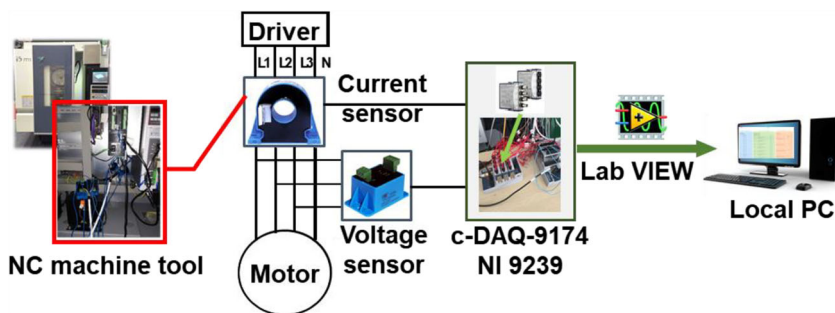
with a correlation coefficient value as high as 0.84 between them. Further, the two transition points could be recognized from the η_2 evolution, which provides a high-precision evaluation of the tool condition. From the above results, it is arrived that the feature η_2, which is extracted from the spindle power signal based on the HHT method, can be used as the index of the tool condition. We suppose that the ability of processing both the nonlinear and nonstationary data of the HHT algorithm attribute to this result significantly.

Due to the changes of cutting parameters, the total numbers of cutting cycles in the first three experiments differed from each other, which were 51, 48, and 39, respectively. Figure 5 shows the results of experiments 2 and 3. The left column represents the changes of η_1. The highly vibrating data make it hard to figure out the relationship between η_1 and VB, nor the transition point of the tool wear region. While in Fig. 5b

and d, the behavior of η_2 is consistent with the tendency of the actual flank wear. In the initial wear stage of experiment 2, the amount of η_2 increases rapidly. Subsequently, η_2 shows a gradually increasing tendency in fluctuation followed by a rapid wear stage, during which the growth rate rises abruptly. In these three experiments, the tool wear conditions are well characterized by the fluctuating η_2. The results demonstrate that the proposed features are independent of cutting parameters in 45 steel machining operation.

Additionally, the correlation coefficient value between the feature and the flank wear increases from 0.37 and 0.50 to 0.79 and 0.93 in these two experiments. It can be explained by the mode mixing problem of the EMD, which results in great difficulty in separating the noise components in the signal through EMD directly. Thus, it is necessary to perform Hilbert transform to extract features more sensitive to the wear state of the cutter.

Fig. 4 The graph of VB and η versus cutting cycle in experiment 1: a η_0, b η_1, c η_2. d The typical growth pattern of tool wear: initial wear region, normal wear region, and rapid wear region
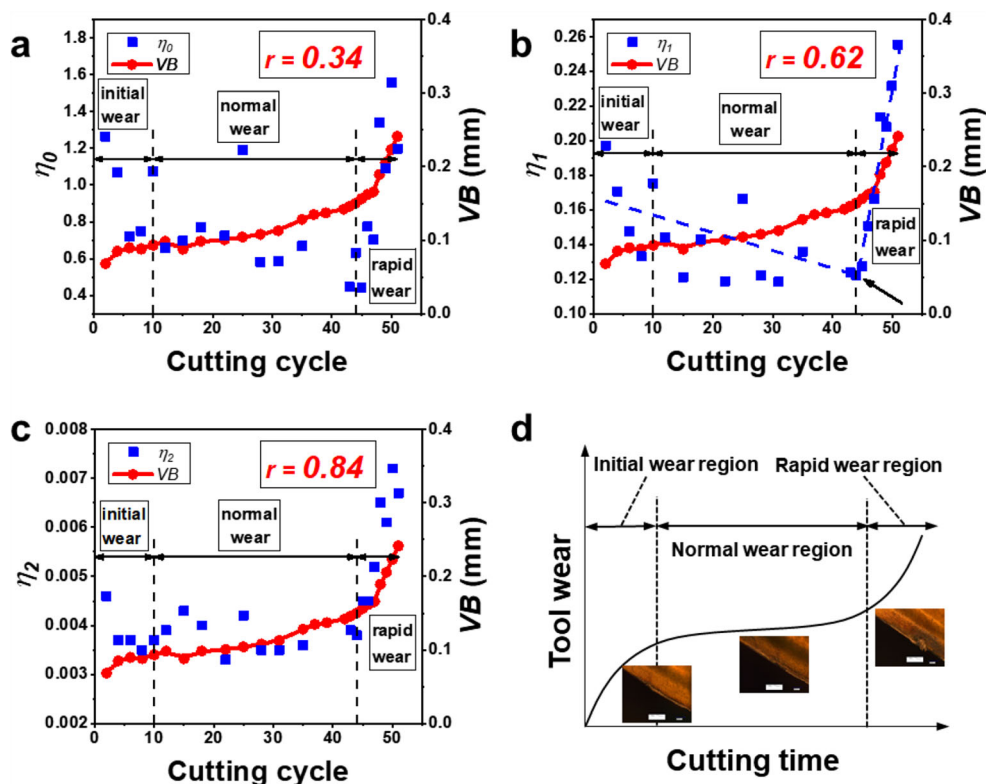
Fig. 5 The graph of VB and η versus cutting cycle: **a** η_1 in experiment 2, **b** η_2 in experiment 2, **c** η_1 in experiment 3, **d** η_2 in experiment 3
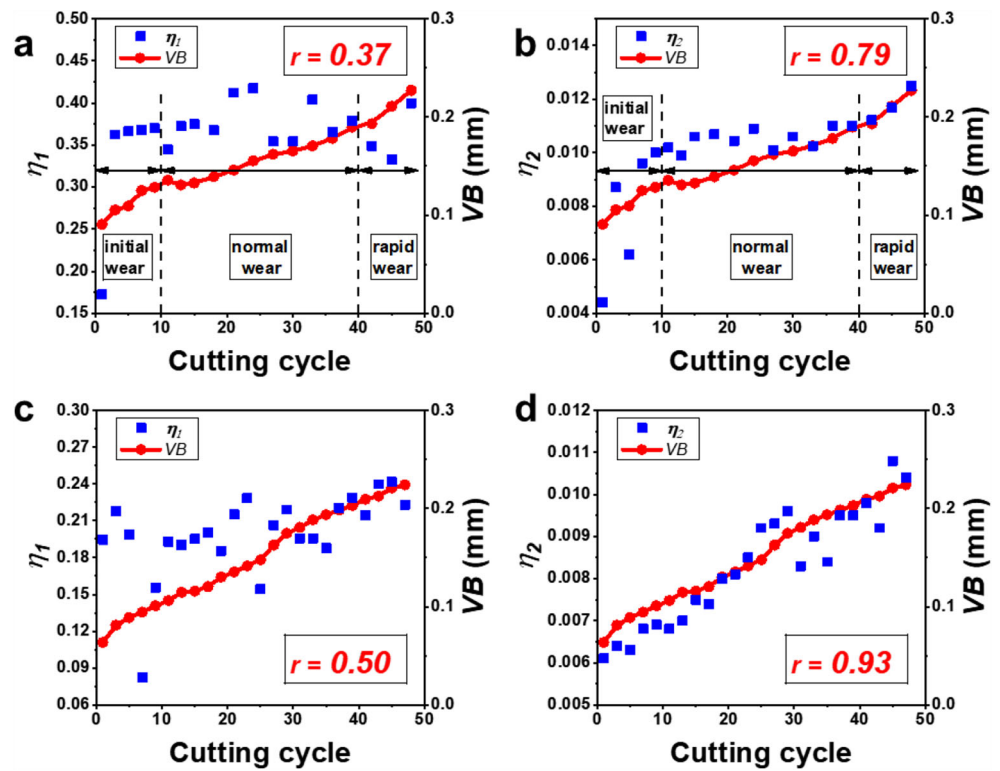

As the TC4 titanium alloy is a difficult-to-machine material, the cutting tools experience severe wear and thus the rapid failure during the cutting process. The accuracy of the HHT-based signal analysis in this cutting condition is verified in experiment 4. In milling TC4, cutting chips started to wrap around the cutting tool at the 11th cycle and the flank wear reached 0.19 mm after 15 cutting cycles. Figure 6 demonstrates the results obtained in experiment 4. In the initial wear stage, the increments of tool wear are too small to be detected and presented in the graph. As it is exhibited in the pictures, in spite of slight oscillations due to the noise disturbance, both η_1 and η_2 have a strong correlation with the actual flank wear. Both correlation coefficients (r) between the η_1 and the measured VB and the η_2 and the measured VB surpassed 0.85, which is different from the results obtained in the previous experiments

that the η_2 exhibits higher correlation coeffect compared with the η_1. During the machining of TC4, the cutting forces change significantly and have more impact on the spindle power because of the rapid increase of built-up edge, the complex tool wear mode and the plastic deformation of cutting edge [29–32]. Therefore, the spindle power signals collected in this condition contain higher proportion of parts related with the tool wear and thus less proportion of noise. In this case, the feature obtained using EMD is accurate enough to estimate the tool wear. According to the correlation coefficient of each test, we could conclude that the workpiece materials has little influence on the accuracy of this analysis method.

By comparing the results obtained from tests of drill TC4 and 45# steel, we showed that influence of the workpiece material on the HHT-based TCM method. Figure 7 a and b present the IMF components and the marginal spectrum of the 106th drilling

Fig. 6 The graph of VB and η versus cutting cycle in experiment 4: **a** η_1, **b** η_2
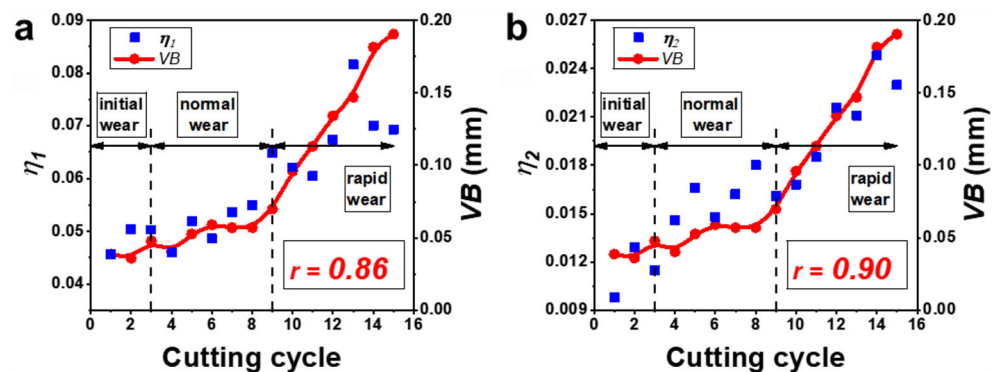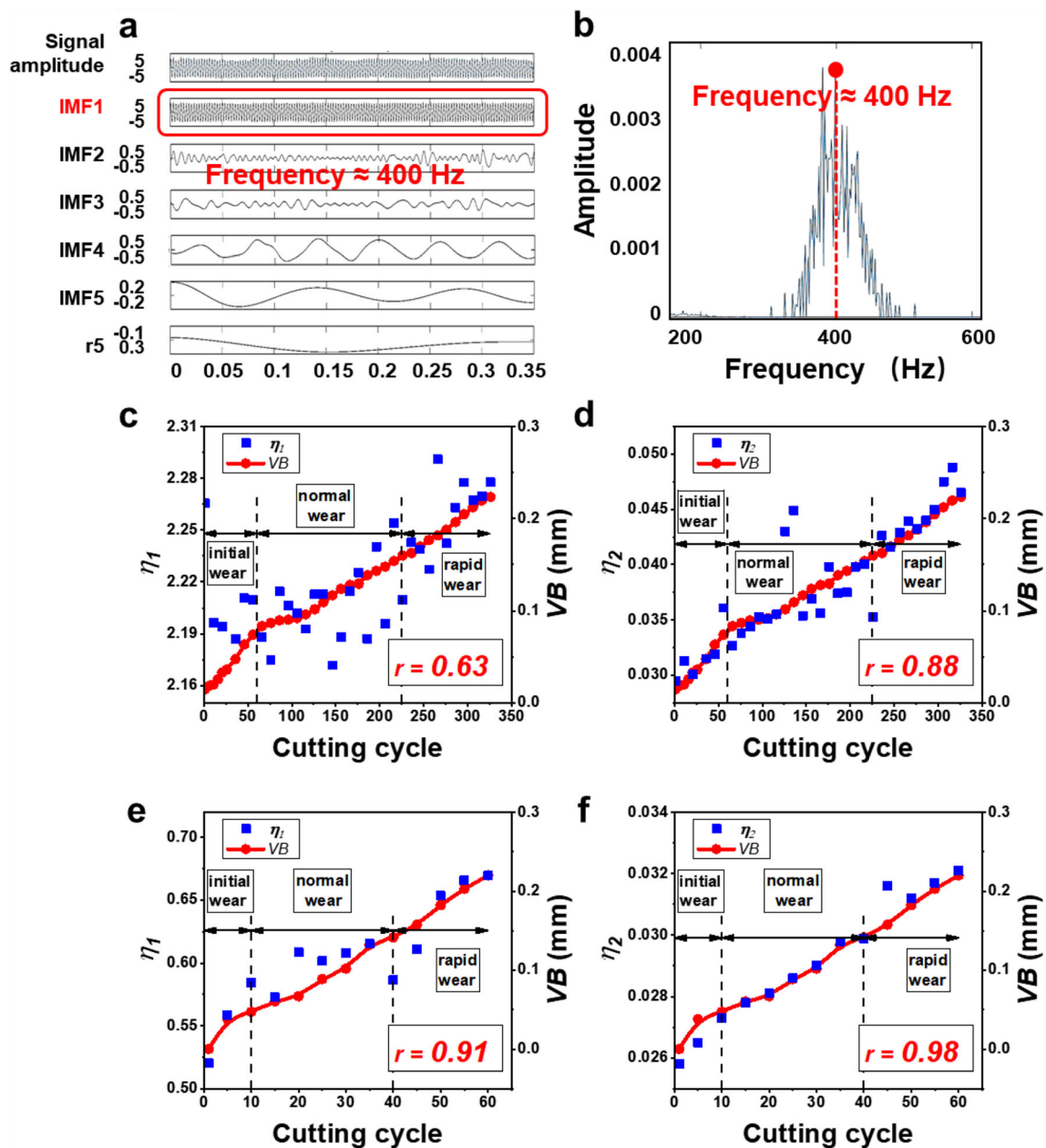
Fig. 7 The HHT processing results of the 106th drilling cycle in experiment 5: **a** IMF components, **b** marginal spectrum. The graph of *VB* and η versus cutting cycle: **c** η_1 in experiment 5, **d** η_2 in experiment 5, **e** η_1 in experiment 6, **f** η_2 in experiment 6

cycle in experiment 5. Since the cutting edges of the drill constantly contacted with the workpiece in the drilling process, f_d is no longer equal to f_t. According to the marginal spectrum in Fig. 7b, the dominant frequency corresponds to 400 Hz. This phenomenon also occurred in experiment 6. Therefore, the IMF component matching 400 Hz is selected as the optimal IMF to calculate η_1.

Figure 7 c and d display the results of experiment 5. As the flank wear of the drill increases, both η_1 and η_2 show an apparent upward trend. In contrast to the highly fluctuating η_1, η_2 stabilized around the curve of *VB* versus cutting cycle and is more sensitive to the tool's condition. The results

presented in Fig. 7e and f further confirm that both the two features (η_1 and η_2) can reflect the wear condition of the drill in drilling TC4. Besides, it is noted that in experiment 6, both the two features closely correlate with the flank wear of the cutting tool, which is consistent to the results obtained in experiment 4.

4 Discussion

Figure 8 displays the cutting edge of the tool after each cutting experiment. In the initial wear stage, we can see an even flank

Fig. 8 Pictures of the tool edge for each experiment, scale bar = 1 mm
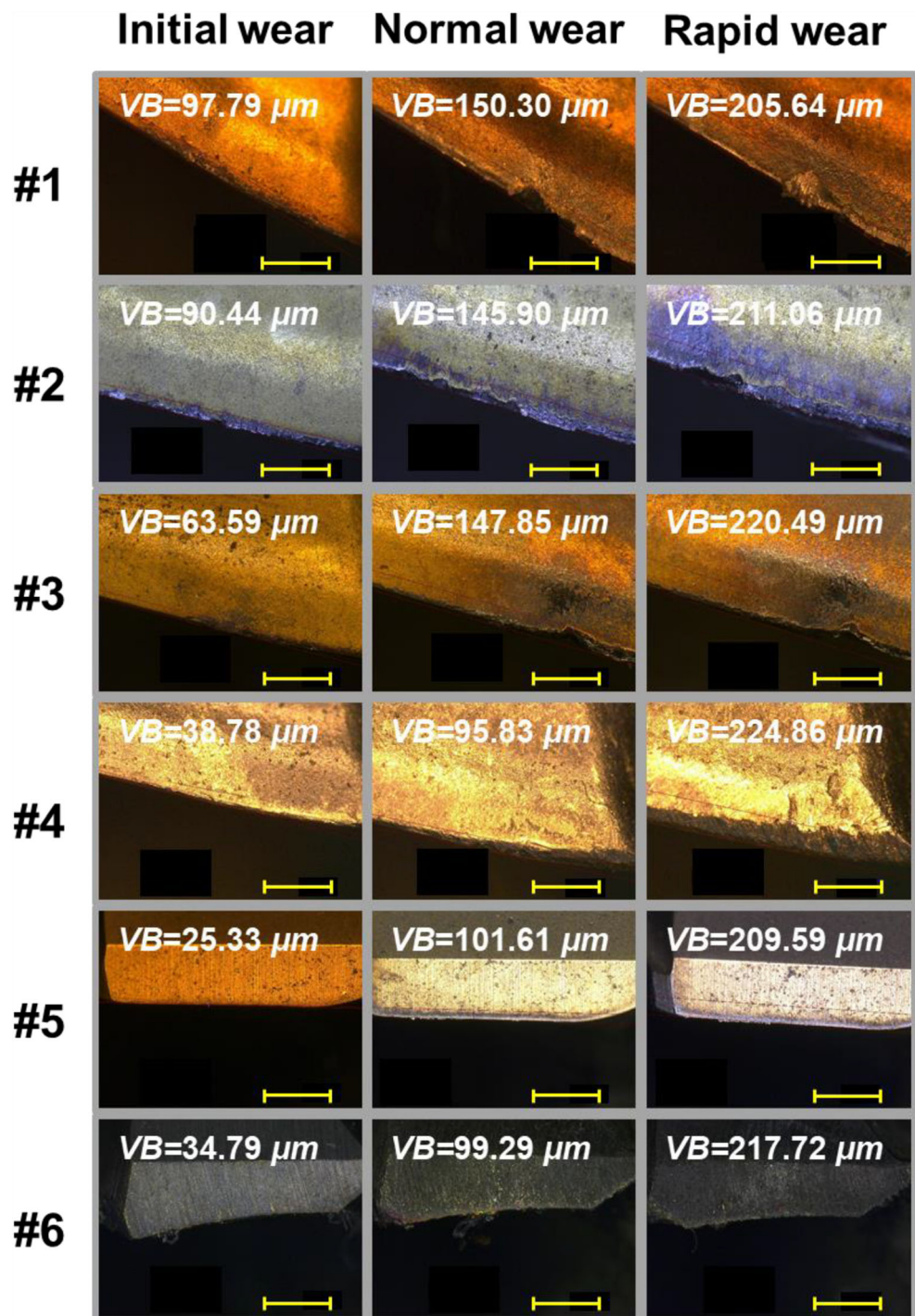
wear of the cutting edge. When the cutting tool entries the normal wear phase, a chipped or blunt cutting edge with uneven wear can be observed.

For us, what makes sense is the moment that the tool entries into the failure region as displayed in Fig. 8. As it is impossible to identify the actual transition point due to the limit of capturing the cutting edge of the tool, instead, we monitor the geometrical changes of the cutting edge by examining the evaluation of the η indirectly.

Table 2 demonstrates the correlation coefficients between the extracted η and the actual flank wear. The following conclusions can be drawn.

In experiment 1, the spindle power signals were analyzed by the CWT and HHT algorithm to extract three features. Although it has been reported that the feature extracted from the spindle power signal based on the CWT algorithm could reflect the tool condition precisely [19], challenges still remain in selecting an appropriate

Table 2 The correlation coefficients between the extracted features and the actual flank wear

Experiment	Method and material	r between η_0 and VB	r between η_1 and VB	r between η_2 and VB
1	Flank milling, 45 steel (parameter 1)	0.34	0.62	0.84
2	Flank milling, 45 steel (parameter 2)	–	0.37	0.79
3	Flank milling, 45 steel (parameter 3)	–	0.50	0.93
4	Flank milling, TC4	–	0.86	0.90
5	Drilling, 45 steel	–	0.63	0.88
6	Drilling, TC4	–	0.91	0.98

wavelet basis function for the detection of a potential unknown tool failure. Comparatively, the HHT algorithm could process both nonlinear and nonstationary signal with a high resolution. Therefore, using the HHT algorithm, the uncertainty of the Wavelet transform could be overcome. The correlation coefficients between the three extracted features and the VB are 0.34, 0.62, and 0.84, among which the η_2 presents the strongest correlation with the flank wear of the cutting tool. These results indicate that the two features (η_1 and η_2) can extract more valuable information that related with the tool condition from the raw signals.

In the present study, the correlation coefficients between the features extracted from the spindle power signal by the HHT algorithm range from 0.79 to 0.98 and they showed weak dependence on the cutting parameters, the workpiece material, or the machining method. That is to say, both the η_1 and η_2 are reliable indicators of the tool wear. Furthermore, the low-cost of the signal acquisition system for the spindle power and the fast and straightforward algorithm developed in the present study to extract features provides a potential application of this method in the real workshop.

Comparing with the η_1 that is extracted from the EMD method, the η_2 shows stronger correlation with the measured flank wear. Even though EMD is theoretically applied to any signal, challenges still remain regarding to the mode mixing in the feature extraction from weak and composite raw signals. Therefore, the Hilbert transform is used to obtain more sensitive features. The inherent property of the HHT method allows observation of the effect of the geometric changes resulted from the tool wear on the marginal spectra with little disturbances. Considering that the calculation of η_2 costs more than 72% higher CPU time than that of η_1, η_1 has an advantage in being able to determine the tool wear stage rapidly and improve the real-time performance of the whole system, and η_2 is suitable to estimate the amount of the tool wear precisely.

Besides, we observe that both the two features in experiment 6 have the strongest correlation with the VB compared with the results obtained in other experiments. The correlation coefficients obtained in experiments 4 and 5 are relatively higher than those obtained in the first three tests. Under different cutting conditions, the signals generated due to the tool wear account for different proportions in raw spindle power data, the complexity of extracting useful features from raw signals varies greatly. Under a complicated machining condition, such as experiments 4 and 6, the response of the spindle power to the cutting tool condition is great enough to be represented by η_1 that is extracted from the EMD method.

5 Conclusion

In the present study, two reliable features are successfully extracted from the spindle power signal using the HHT algorithm to precisely estimate the tool condition. The results show that the HHT algorithm can effectively suppress the noise interference in the raw spindle power signal and the extracted two features (η_1 and η_2) consistently coincides with the measured flank wear (VB) of the cutting tool. The correlation coefficients between them calculated in various cutting experiments maintain at a high level and show weak dependence on the cutting parameter, the workpiece material, or the machining method. Besides, the spindle power signal acquisition system could be established at a low cost and the features could be extracted efficiently, which makes such as tool condition monitoring (TCM) system meets the economic and efficiency requirements in the industrial production. For the feasibility of this method in a wider range of cutting tools and machining conditions, further work is required to develop an AI-based monitoring system that can predict tool wear state and promote the efficiency of the management of the tool life cycle.

References

1. Liu Z, Li X, Wu D, Qian Z, Feng P, Rong Y (2019) The development of a hybrid firefly algorithm for multi-pass grinding process optimization. J Intell Manuf 30:2457–2472

2. Liu H, He Y, Mao X, Li B, Liu X (2017) Effects of cutting conditions on excitation and dynamic stiffness in milling. Int J Adv Manuf Technol 91:813–822

3. Santos MC, Machado AR, Sales WF, Barrozo MAS, Ezugwu EO (2016) Machining of aluminum alloys: a review. Int J Adv Manuf Technol 86:3067–3080

4. Guo P, Zou B, Huang C, Gao H (2017) Study on microstructure, mechanical properties and machinability of efficiently additive manufactured AISI 316L stainless steel by high-power direct laser deposition. J Mater Process Technol 240:12–22

5. Li X, Lu Y, Li Q, Li F, Rong YK (2013) The study on the influences of superabrasive grain spatial orientation for microcutting processes based on response surface methodology. Int J Adv Manuf Technol 67:1527–1536

6. Li X, Wolf S, Zhi G, Rong Y (2014) The modelling and experimental verification of the grinding wheel topographical properties based on the 'through-the-process' method. Int J Adv Manuf Technol 70:649–659

7. Feng J, Wan M, Gao T, Zhang W (2018) Mechanism of process damping in milling of thin-walled workpiece. Int J Mach Tool Manu 134:1–19

8. Agmell M, Ahadi A, Gutnichenko O, Stahl J (2017) The influence of tool micro-geometry on stress distribution in turning operations of AISI 4140 by FE analysis. Int J Adv Manuf Technol 89:3109–3122

9. Tian C, Li X, Zhang S, Guo G, Wang L, Rong Y (2018) Study on design and performance of metal-bonded diamond grinding wheels fabricated by selective laser melting (SLM). Mater Des 156:52–61

10. Nouni M, Fussell BK, Ziniti BL, Linder E (2015) Real-time tool wear monitoring in milling using a cutting condition independent method. Int J Mach Tool Manu 89:1–13

11. Ghosh N, Ravi YB, Patra A, Mukhopadhyay S, Paul S, Mohanty AR, Chattopadhyay AB (2007) Estimation of tool wear during CNC milling using neural network-based sensor fusion. Mech Syst Signal Process 21:466–479

12. Kalvoda T, Hwang Y (2010) A cutter tool monitoring in machining process using Hilbert-Huang transform. Int J Mach Tool Manu 50:495–501

13. Zhou Y, Xue W (2018) Review of tool condition monitoring methods in milling processes. Int J Adv Manuf Technol 96:2509–2523

14. Sevilla-Camacho PY, Robles-Ocampo JB, Muniz-Soria J, Lee-Orantes F (2015) Tool failure detection method for high-speed milling using vibration signal and reconfigurable bandpass digital filtering. Int J Adv Manuf Technol 81:1187–1194

15. Pechenin VA, Khaimovich AI, Kondratiev AI, Bolotov MA (2017) Method of controlling cutting tool wear based on signal analysis of acoustic emission for milling. Procedia Eng 176:246–252

16. Hong Y, Yoon H, Moon J, Cho Y, Ahn S (2016) Tool-wear monitoring during micro-end milling using wavelet packet transform and Fisher's linear discriminant. Int J Precis Eng Manuf 17:845–855

17. Li T, Zhang D, Luo M, Wu B (2017) Tool wear condition monitoring based on wavelet packet analysis and RBF neural network. In: International Conference on Intelligent Robotics and Applications. Springer, Cham, pp 388–400

18. Huang NE, Shen SS (2005) Hilbert-Huang transform and its applications. World Scientific

19. Shao H, Shi X, Li L (2011) Power signal separation in milling process based on wavelet transform and independent component analysis. Int J Mach Tool Manu 51:701–710

20. Choi Y, Narayanaswami R, Chandra A (2004) Tool wear monitoring in ramp cuts in end milling using the wavelet transform. Int J Adv Manuf Technol 23:419–428

21. Huang NE, Shen Z, Long SR, Wu M, Shih HH, Zheng QN, Yen NC et al (1998) The empirical mode decomposition and the Hilbert spectrum for nonlinear and non-stationary time series analysis. Proceedings of The Royal Society A-Mathematical Physical and Engineering Sciences 454:903–995

22. Bassiuny AM, Li X (2007) Flute breakage detection during end milling using Hilbert-Huang transform and smoothed nonlinear energy operator. Int J Mach Tool Manu 47:1011–1020

23. Raja JE, Kiong LC, Soong LW (2013) Hilbert-Huang transform-based emitted sound signal analysis for tool flank wear monitoring. Arab J Sci Eng 38:2219–2226

24. Sun H, Niu W, Wang J (2015) Tool wear feature extraction based on Hilbert-Huang transformation. Journal of Vibration & Shock 34(4):158–164 and 182

25. Tansel IN, Mekdeci C, Rodriguez O, Uragun B (1993) Monitoring drill conditions with wavelet based encoding and neural networks. Int J Mach Tool Manu 33(4):559–575

26. Li XL, Tso SK, Wang J (2000) Real-time tool condition monitoring using wavelet transforms and fuzzy techniques. Ieee Transactions on Systems Man and Cybernetics Part C-Applications and Reviews 30:352–357

27. Yesilyurt I (2006) End mill breakage detection using mean frequency analysis of scalogram. Int J Mach Tool Manu 46:450–458

28. Walker B, Panda J, Sutliff D (2008) Vibration analysis of the space shuttle external tank cable tray flight data with and without PAL Ramp. Aiaa Aerospace Sciences Meeting & Exhibit

29. Sun S, Brandt M, Mo JPT (2014) Evolution of tool wear and its effect on cutting forces during dry machining of Ti-6Al-4V alloy. Proceedings of the Institution of Mechanical Engineers Part B-Journal of Engineering Manufacture 228:191–202

30. Wang Y, Zou B, Huang C (2019) Tool wear mechanisms and micro-channels quality in micro-machining of Ti-6Al-4V alloy using the Ti(C7N3)-based cermet micro-mills. Tribol Int 134:60–76

31. Fu X, Zou B, Liu Y, Huang C, Yao P (2019) Edge micro-creation of Ti(C, N) cermet inserts by micro-abrasive blasting process and its tool performance. Machining Sci Technol 23(5)

32. Wang Y, Zou B, Wang J, Wu Y, Huang C (2020) Effect of the progressive tool wear on surface topography and chip formation in micro-milling of Ti–6Al–4V using Ti(C7N3)-based cermet micro-mill. Tribol Int 141:105900